ChemSusChem

Research Article
doi.org/10.1002/cssc.202300995

Chemistry Europe
European Chemical Societies Publishing

www.chemsuschem.org

# Unraveling Propylene Oxide Formation in Alkali Metal Batteries

Daniel Stottmeister,*[a] Leonie Wildersinn,*[b] Julia Maibach,*[b, c] Andreas Hofmann,*[b] Fabian Jeschull,*[b] and Axel Groß*[a, d]

The increasing need for electrochemical energy storage drives the development of post-lithium battery systems. Among the most promising new battery types are sodium-based battery systems. However, like its lithium predecessor, sodium batteries suffer from various issues like parasitic side reactions, which lead to a loss of active sodium inventory, thus reducing the capacity over time. Some problems in sodium batteries arise from an unstable solid electrolyte interphase (SEI) reducing its protective power e.g., due to increased solubility of SEI components in sodium battery systems. While it is known that the electrolyte affects the SEI structure, the exact formation mechanism of the SEI is not yet fully understood. In this study, we follow the initial SEI formation on a piece of sodium metal submerged in propylene carbonate with and without the electrolyte salt sodium perchlorate. We combine X-ray photoelectron spectroscopy, gas chromatography, and density functional theory to unravel the sudden emergence of propylene oxide after adding sodium perchlorate to the electrolyte solvent. We identify the formation of a sodium chloride layer as a crucial step in forming propylene oxide by enabling precursors formed from propylene carbonate on the sodium metal surface to undergo a ring-closing reaction. Based on our combined theoretical and experimental approach, we identify changes in the electrolyte decomposition process, propose a reaction mechanism to form propylene oxide and discuss alternatives based on known synthesis routes.

## Introduction

Electrochemical energy storage in batteries is crucial for successfully transitioning from fossil fuel usage to a sustainable energy economy.[1] Lithium-ion batteries (LIBs) exhibit a high energy density and operating voltage while maintaining a sufficiently long cycle life. Thus, LIBs have established themselves as the prime non-stationary energy storage solution.[2] However, LIBs cannot store the inexorably increasing energy needed for today's society for various reasons. Not the least of these reasons is the relative scarcity of lithium in the earth's crust and its uneven global distribution, combined with the environmentally unfriendly mining process.[3] It is, therefore, essential to diversify energy storage beyond lithium. One of the most promising alternatives to lithium batteries are sodium batteries[5,6] which, unlike lithium, do not suffer from scarcity issues due to sodium's relative abundance. Based on sodium's chemically similar behavior to lithium, many concepts developed through the study of lithium batteries can be applied to sodium batteries.[7,8]

One such aspect lies in understanding the solid electrolyte interphase (SEI) formation. Although there are differences due to different kinds of anode materials used between lithium and sodium-based batteries (graphite versus hard carbon), the SEI is a crucial component for the functionality and safety of alkali batteries and has been studied extensively using experimental and theoretical methods.[9] It has been demonstrated that the electrolyte composition significantly impacts SEI formation. Numerous studies have shown the importance of the solvent mixture,[10–12] as well as the used electrolyte salt.[13,14] Further, the beneficial effects of additives like FEC or VC on the stability of the SEI have been established.[15–18] Therefore, all electrolyte components contribute to the formation of the SEI, the salt, the charge carrier, the solvent, and the additives.[19,20] However, the mechanisms through which the different components influence the growth of the SEI still need to be fully understood.

Resolving said mechanisms has been the focus of many studies, ranging from atomistic simulations to experimental

[a] D. Stottmeister, Prof. Dr. A. Groß
Institute of Theoretical Chemistry, Ulm University
89069 Ulm, Germany
E-mail: daniel.stottmeister@uni-ulm.de
axel.gross@uni-ulm.de

[b] L. Wildersinn, J. Maibach, A. Hofmann, F. Jeschull
Karlsruher Institut für Technologie,
Institut für Angewandte Materialien (IAM)
Herrmann-von-Helmholtz Platz 1,
76344 Eggenstein – Leopoldshafen, Germany
E-mail: leonie.wildersinn@kit.edui
julia.maibach@chalmers.se
andreas.hofmann2@kit.edui
fabian.jeschull@kit.edui

[c] J. Maibach
Department of Physics, Chalmers University of Technology
SE – 412 96 Gothenburg, Sweden
E-mail: julia.maibach@chalmers.se

[d] Prof. Dr. A. Groß
Helmholtz Institute Ulm (HIU) Electrochemical Energy Storage
Helmholtzstr. 11, 89069 Ulm, Germany
E-mail: axel.gross@uni-ulm.de

Supporting information for this article is available on the WWW under https://doi.org/10.1002/cssc.202300995

post-mortem analysis.[21–24] The complexity of the SEI poses a challenge for both, experimentalists and theoreticians alike. Combining the different sizes and timescales often complicates any direct comparison between the atomistic view of theoretical simulations, which typically operate on the picosecond timescale, and the macroscopic scale of experiments, which frequently operate on timescales spanning days or weeks. Here, we attempt to unravel one piece of the puzzle: the influence of sodium perchlorate on the SEI formation in sodium (metal) batteries using propylene carbonate as the electrolyte solvent. We combine atomistic scale density functional theory (DFT) and *ab initio* molecular dynamics (AIMD) simulations with X-ray photoelectron spectroscopy (XPS) and gas chromatography (GC) measurements to develop a detailed understanding of the initial SEI formation steps in this system.

## Results and Discussion

### Electrolyte decomposition products

In this study, we expand upon the previous work of Hofmann et al., where the reactivity of different electrolyte compositions on sodium metal was tested extensively.[25] Here, we utilize DFT calculations to better understand the electrolyte decomposition process by calculating the thermodynamic stability of possible fragments and comparing these results to the established experimental data. In the first step, we screened the adsorption energies of hypothesized decomposition products on surfaces likely to exist at the metal-electrolyte interface. A compilation of the considered decomposition products is illustrated in Figure 1. This step is essential when comparing theoretical results with experimental data in order to consider the detectability of potential decomposition products to understand electrolyte decomposition based on gas phase analysis. Any decomposition product which strongly bonds to the electrode surface (adsorption energy $\gg 1$ eV) will be unable to desorb into the electrolyte under room temperature conditions and will, therefore, be undetectable within the scope of gas phase analysis methods.

All electrolyte decomposition products were derived from dimethyl carbonate (DMC), ethylene carbonate (EC), or propylene carbonate (PC) as a base. We considered the surface terminations with the three lowest surface energies of pure sodium and the (100) and the (111) surfaces of sodium chloride.

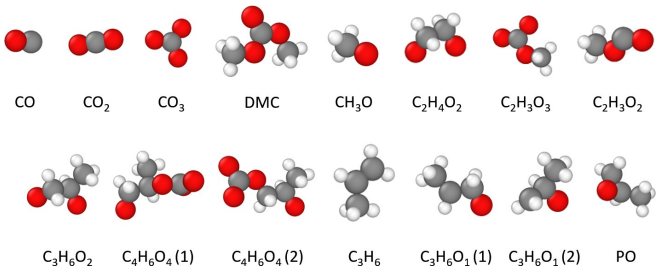


**Figure 1.** Illustration of the investigated possible electrolyte decomposition products.

We considered both the NaCl(100) and the NaCl(111) surfaces since whereas the NaCl(100) surface is known to be the most stable NaCl surface,[26] the NaCl(111) surface has been observed in several instances.[27,28] We specifically consider the Na-rich NaCl(111) due to its resemblance to Na-metal. These surface terminations should be stabilized at high Na electrochemical potentials[29] or rather low Cl potentials, as the sum of these two potentials is fixed by the chemical potential of NaCl salt. We calculated the adsorption energy using:

$$E_{ads} = E_{adsorbed} - E_{adsorbate} - E_{surf} \quad (1)$$

To make our study fully comprehensible to both experimentalists and theoreticians alike, we like to briefly address the topic of semantics concerning the adsorbates used within this work. All calculations were performed in charge-neutral systems. First of all, in equilibrium the electric double layer (EDL) at electrochemical interfaces is necessarily charge-neutral because otherwise electric fields would result that eventually cause charge neutrality.[30] Second, upon adsorption the adsorbate becomes part of the electronic system of the electrode which in principle acts as an electron reservoir. Finite-size effects due to the slab model used in the periodic set-up have been controlled through making sure that the adsorption properties are converged with respect to the slab thickness. Therefore we describe the carbonate adsorbate as $CO_3$ since no additional charges are introduced into the system. This does, however, not imply that the carbonate moiety is charge neutral after adsorption on the respective surface. All calculated adsorption energies are listed in the Table 1.

Propylene oxide (PO) as well as CO and $CO_2$ exhibit low adsorption energies on both the metal and the chloride surface, leading to a significant amount of these molecules that do not stay at the surface, thus enabling gas phase analysis methods to detect their presence. Similarly, unreacted DMC, as well as any formed propene, should also be detectable. Many of the investigated decomposition products, such as $[CO_3]^{-2}$ and propandiolate are found to chemisorb on the sodium and the (111) sodium chloride surfaces, likely causing them to be invisible for the experimental gas phase analysis. Therefore, gas phase analysis methods will be ill-suited to detect many of these "first step" products.

In the following, we will take a closer look into how the compounds adsorb on the considered surfaces, focusing on adsorbates that show a substantial variation in their adsorption behavior on these surfaces. First, we look at carbon monoxide, which offers little difference in adsorption energy between sodium metal and sodium chloride. Despite this slight difference in energetics, the adsorption of CO on sodium chloride occurs via a Na–O binding, in contrast to the Na–C binding on metallic sodium, which is well established for other metal surfaces.[31] The different adsorption structures for CO and $CO_2$ are depicted in Figure 2.

While from a strictly energetical perspective, there is little difference between the chloride and the metal surface for CO adsorption, for $CO_2$ we noticed a significant increase in the adsorption energy on the NaCl(111) surface. Its stronger

**Table 1.** Calculated adsorption energies for proposed decomposition products and educts on different surface cuts of Na and NaCl.

| | Na(100) | Na(110) | Na(111) | NaCl(100) | NaCl(111) |
|---|---|---|---|---|---|
| CO | −0.25 eV | −0.26 eV | −0.23 eV | −0.17 eV | −0.42 eV |
| $CO_2$ | −0.25 eV | −0.19 eV | −0.19 eV | −0.35 eV | −2.02 eV |
| $CO_3$ | −8.24 eV | −7.98 eV | −7.90 eV | −0.88 eV | −8.96 eV |
| DMC | −0.57 eV | −0.56 eV | −0.48 eV | −0.47 eV | −1.22 eV |
| $CH_3O$ (methanolate) | – | −3.59 eV | – | −0.42 eV | −4.06 eV |
| $C_2H_4O_2$ (1,2-ethandiolate) | −4.00 eV | −3.74 eV | −3.94 eV | −0.60 eV | −4.66 eV |
| $C_2H_3O_3$ (methyl carbonate) | −4.65 eV | −4.53 eV | −4.61 eV | −0.50 eV | −5.30 eV |
| $C_2H_3O_2$ (methoxymethanolate) | −2.46 eV | −2.59 eV | −2.38 eV | −0.48 eV | −3.49 eV |
| $C_3H_6O_2$ (1,2-propandiolate) | −3.90 eV | −3.74 eV | −3.94 eV | −0.60 eV | −0.46 eV |
| $C_4H_6O_4$ (1) | −8.14 eV | −7.92 eV | −7.81 eV | −0.69 eV | −9.24 eV |
| $C_4H_6O_4$ (2) | −7.28 eV | −7.10 eV | −3.46 eV* | −0.65 eV | −9.19 eV |
| $C_3H_6$ (propene) | −0.11 eV | −0.24 eV | −0.27 eV | −0.37 eV | −0.50 eV |
| $C_3H_6O_1$ (1) (1-propanolate-2-yl) | −0.76 eV | −0.66 eV | −1.00 eV | −0.49 eV | −0.87 eV |
| $C_3H_6O_1$ (2) (2-propanolate-1-yl) | −1.86 eV | −1.94 eV | −2.02 eV | −0.51 eV | −2.84 eV |
| PO (propylene oxide) | −0.42 eV | −0.43 eV | −0.14 eV | −0.51 eV | −0.93 eV |

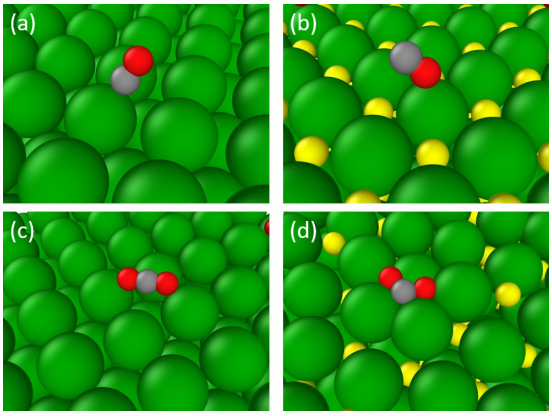


**Figure 2.** Comparison of adsorption positions for (a) CO on Na(100), (b) CO on NaCl(100), (c) $CO_2$ on Na(100) and (d) $CO_2$ on NaCl(111). Oxygen is depicted in red, carbon in grey and chlorine in yellow.

adsorption on NaCl(111) is further reflected in its modified adsorption structure (see Figure 2d), in which the $CO_2$ molecule is no longer linear. This indicates a significant change in the bonding structure of the molecule, with the C atom bound to the top layer sodium atoms. This bend $CO_2$ structure is similar to the adsorption of $CO_2$ on stepped transition metal surfaces.[32] A Bader charge analysis further proves the reduction of the carbon atom where in the $CO_2$ molecule on the sodium surfaces, the carbon atom has a charge of +4, and the carbon on the NaCl(111) surface has a reduced charge of +1.8. According to our calculations, the sodium-rich NaCl surface is more reactive than the Na metal surfaces, leading to several tightly bonded adsorbates on this specific surface. When comparing the adsorption of carbon monoxide and carbon dioxide with carbonate adsorption, we found that carbonate adsorbs significantly stronger on both metallic sodium and sodium chloride. The only surface on which carbonate adsorbs reversibly was the NaCl(100) surface. A direct structural comparison between the $[CO_3]^{-2}$ adsorption between the sodium metal and sodium chloride surfaces is shown in Figure 3. Carbonate is firmly bound on the metal and the NaCl(111) surface, with all oxygen atoms coordinating Na atoms. However, in the case of the NaCl(100) surface, the $[CO_3]^{-2}$ fragment stands upright with only two oxygen atoms coordinating with Na surface atoms. The much lower adsorption energy for the NaCl(100) surface can be explained by the carbonate's reluctance to bind to chloride atoms, which comprise a significant portion of the NaCl(100) top surface layer.

Finally, we observed the strong chemisorption of propandiolate, a decomposition product of PC, originating from the CO forming reaction,[33] on all surfaces except the NaCl(100) surface. The diolate was unstable on the NaCl(100) surface instead and decomposed into formaldehyde and acetaldehyde, as depicted in Figure 4. After establishing the thermodynamic stability and adsorption behavior of a selection of potential decomposition products, we now focus on one specific system consisting of PC, either with or without sodium perchlorate salt as the electrolyte mixture in contact with a sodium metal surface. Note that we have used perchlorate salt as it has been successfully employed in a previous study[25] in spite of the fact that safety concerns prevent upscaling for commercial use.[34] We first report the experimental findings using GC measurements.

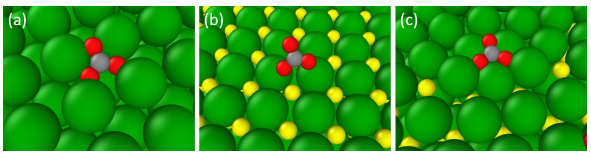


**Figure 3.** Comparison of adsorption positions for (a) $CO_3$ on Na(100), (b) $CO_3$ on NaCl(100) and (c) $CO_3$ on NaCl(111).

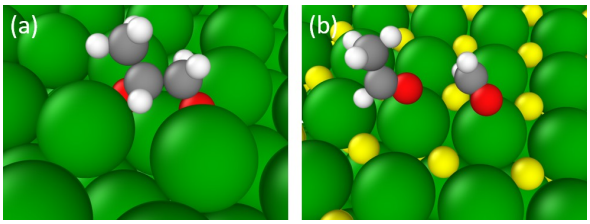


**Figure 4.** Comparison of adsorption positions for (a) Propanolate on Na(100), (b) Propanolate on NaCl(100).

## Gas Chromatography

We analyzed the gases according to the previously described procedure.[25] Shortly, the liquid electrolyte and sodium metal pieces were placed in a sealed cell container where pressure as well as gas could be determined/extracted. A photograph of the cell and a schematic drawing of the setup are shown in Figure 5 for a better illustration of the measurement.

We could confirm in repeated measurements that a pressure increase within 800 h only takes place when $NaClO_4$ is present. The pressure inside the cell remains almost constant when propylene carbonate and Na metal are available. Additionally, it was observed that the propylene carbonate becomes a yellowish high-viscous compound over time. This effect results from polymerization reactions that take place between Na metal and PC. Such reactions were seen with and without $NaClO_4$ as conducting salt. When $NaClO_4$ is present, propylene oxide, as well as hydrogen and carbon monoxide, were detected in significant amounts (see also Figure S24 in Ref. [35]). Additionally, we could see propene as well as propylene oxide in the MS gas measurement (Figure 6). Note that the PO signal appears to be very weak. However, we performed additional measurements with a more sensitive GC mass spectrometer (not shown in Figure 6) that was not used standardly as it does not allow a gas separation for gases and alkanes with low C-numbers. These measurements yielded a significantly increased PO intensity. The formation of propene, which was assigned by NIST data evaluation with high data match (940/1000), is proposed analogously for ethylene in EC-based electrolyte mixtures[36] and could be confirmed in this study in case of PC based electrolytes experimentally.

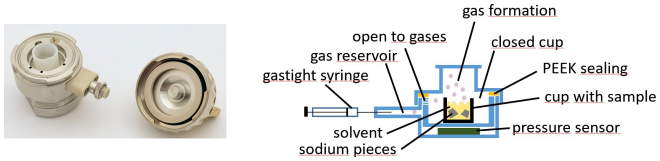


**Figure 5.** Photograph (left hand side) as well as schematic drawing (right hand side) of the gas formation setup including the description of the individual parts.

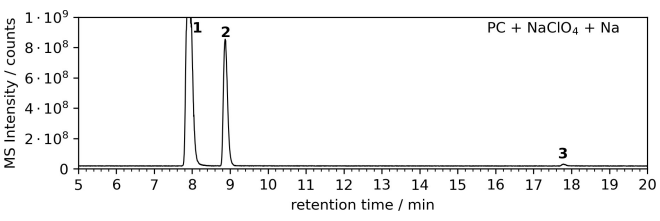


**Figure 6.** GC-MS chromatogram from the gas measurement of PC + $NaClO_4$ + Na mixture after 1 week. Compound 1: air/Ar/CO, 2: propene, 3: propylene oxide.

## PO Formation Mechanism

To understand the sudden formation of PO in the perchlorate-containing setup, we must first investigate the $[ClO_4]^-$ interaction with sodium metal. Analogous to previous results for the perchlorate decomposition on lithium metal, we observed the reaction of $[ClO_4]^-$ with sodium metal during an AIMD simulation run in which, similar to the lithium simulations, the chloride atoms stayed in the top layer of the sodium metal, while the oxygen atoms sunk deeper into the surface.[33] This formation of a chloride-rich surface layer represents a significant difference between the perchlorate-free and perchlorate-containing systems. We hypothesize that this formation of a sodium-chloride layer can explain the sudden emergence of PO in the gas phase. To test this hypothesis, we investigated three atomistic properties necessary for detecting PO in our GC measurements, the thermodynamic stability of PO on the respective surfaces, the adsorption energy of PO on a NaCl surface, and the reaction pathway for the formation of PO. We performed AIMD simulations to determine the stability of PO on the sodium-metal/sodium-chloride surface and found that PO follows a ring-opening reaction only on the sodium surface.

In contrast, the PO molecule on the NaCl surface remained intact. Structure optimization calculations for PO and the ring-opening product on Na and the NaCl surfaces yield that the ring-opening reaction is exothermic on sodium metal, while it is endothermic on the NaCl surface. Hence, the NaCl surface stabilizes the PO molecule. Apart from the thermodynamic stability, PO must not bind strongly to the NaCl surface to be detectable by GC measurements. We compared the adsorption energies of PO on the NaCl surfaces with the adsorption energy on the sodium metal surfaces and found PO to bind with energies below 1 eV on all tested surfaces consistently; the optimized structures are depicted in Figure 7. The low adsorption energy implies that if PO is formed on the NaCl surface, it should be detectable via GC, assuming it is not trapped within the liquid electrolyte mixture.

After verifying PO's stability and detectability, its formation mechanism still needs to be clarified. With PC as the educt, one

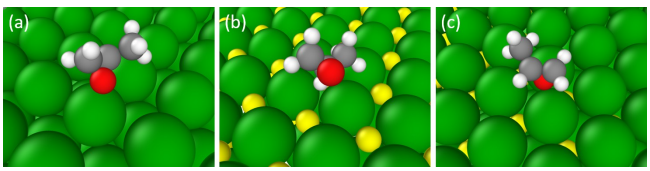


**Figure 7.** Comparison of adsorption positions for (a) PO on Na(100), (b) PO on NaCl(100) and (c) PO on NaCl(111).

could imagine several possible reaction pathways leading to the formation of PO. Figure 8 shows a comparison between the assumed most relevant decomposition products for the PO formation. $[CO_3]^{-2}$ and propandiolate are found to chemisorb on all sodium and the (111) sodium chloride surface, which is probably the cause that they are invisible for the experimental gas phase analysis. Based on the experimental GC results, in which we did not detect any $CO_2$, and our adsorption calculations, which suggest that any $CO_2$ that is formed should be detectable, we can assume that no $CO_2$ is involved in the PO reaction, while CO is abundant. Our previous computational study identified a CO-producing decomposition reaction in which PC would decompose into propandiolate and CO.[33] CO was readily detected within the GC experiments while propandiolate chemisorbs on the Na surface, likely making it undetectable within our measurement. Assuming a CO-induced ring-opening of propylene carbonate is the first step, we start with the $C_4H_6O_4$ molecule. This reaction has been observed in our AIMD simulations for ethylene carbonate on lithium as depicted in Figure 9, where the readily formed CO performs a nucleophilic attack on the carbonate carbon of an EC molecule resulting in a ring-opening reaction,[37] leading to the formation of $C_3H_3O_4$ and carbon.

The dissociation of CO into oxygen and elemental carbon on lithium surfaces has been previously observed.[38] In fact, almost all organic molecules can decompose on lithium surfaces, as verified in computational studies.[39,40] As sodium (and in particular potassium) exhibit an even higher reactivity compared to lithium, we also expect a similar decomposition behavior on Na compared to Li. The formation of ethylene oxide, the EC analogous to our PO, has previously been detected for perchlorate-containing lithium systems, although a different reaction mechanism was proposed.[41]

Notably, the $C_3H_3O_4$ molecule might also function as a precursor to the well-established common SEI component ethylene dicarbonate.[42] While we did not observe the CO-induced ring opening reaction for PC directly due to the chemical similarities between EC and PC and the carbonate group being the active part in this reaction, we suggest this reaction should occur with PC as well as EC. Figure 10 shows the two different isomers of the $C_4H_6O_4$ molecule on the Na(100) surface. While both isomers have almost the same heat of formation (difference $< 0.02$ eV), due to the position of the methyl group, one isomer adsorbs significantly stronger on the sodium surface.

These molecules can easily be cleaved along a C–O bond to allow for the formation of sodium carbonate, as well as the proposed precursor to PO. We chose this reaction as the initial step of the PO formation because the formation of sodium carbonate was previously found to be favorable.[33,43] While we did not detect any $CO_3$ within the GC measurements, Figure 8 shows that any formed carbonate would bind tightly to the metal surface, making it undetectable. At this point, the position of the methyl group, while irrelevant to the final product, may strongly influence the intermediate products. We, therefore, investigated the two possible methyl group placements in reactions a) and b), as visualized in Figure 11.

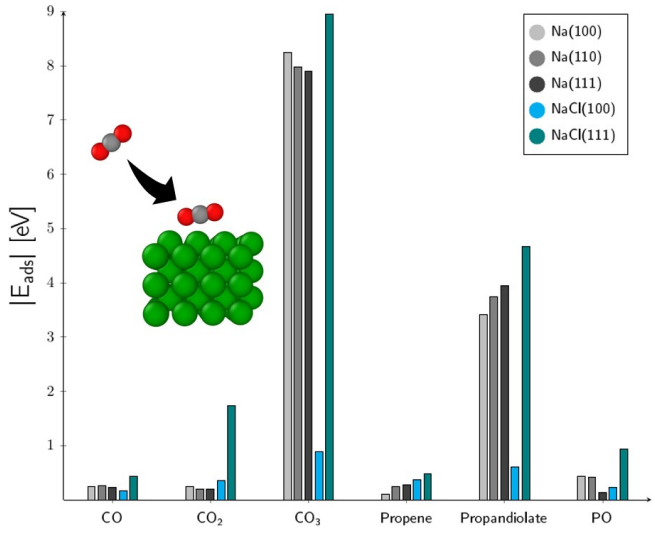


**Figure 8.** Comparison between the adsorption energies of molecules suspected to be involved in PO formation on sodium and sodium chloride surfaces.

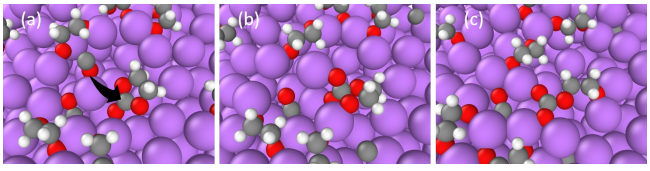


**Figure 9.** Observed formation reaction of $C_3H_3O_4$ on a Li(100) surface. a) CO, the product of the EC decomposition, initiates a nucleophilic attack on the carbonate carbon of EC. b) $CO_4$ Reaction intermediate. c) Ring-opening and $C_3H_3O_4$ formation.

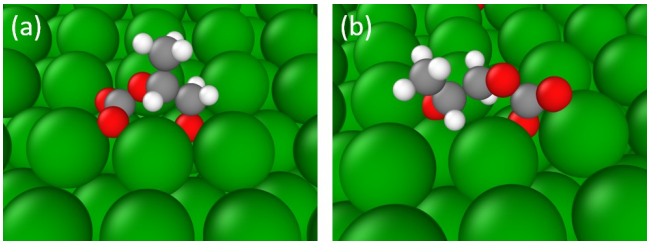


**Figure 10.** Illustration of the two different $C_4H_6O_4$ molecules on the Na(100) surface. a) $C_4H_6O_4$ with the methyl group next to the carbonate group adsorbs strongly (−8.1 eV)) on the Na(100) surface. b) $C_4H_6O_4$ with the methyl group further away from the carbonate group adsorbs less strongly (−7.3 eV) on the Na(100) surface.

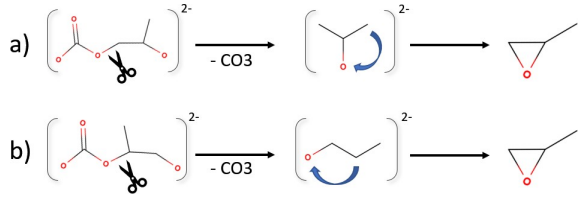


**Figure 11.** Two proposed reaction pathways for the formation of propylene oxide. Please note, that this is a schematic representation in a simplified manner.

To test our hypothesis of PO forming on the NaCl surface, we calculated the thermodynamics of both reaction pathways under vacuum conditions, on the sodium and on the sodium chloride surfaces. We determined the reaction energies according to:

$$E_{reaction} = E_{products} - E_{educt} \quad (2)$$

where $E_{products}$ and $E_{educt}$ refer to the energies of the educts and products in vacuum or the adsorbed molecules on the surface.

Under vacuum conditions, we find no single step in either reaction pathway to be exothermic. The initial $[CO_3]^{-2}$ formation step, while endothermic for both paths, required significantly more energy in the case of pathway a) (1.2 eV) compared to b) (0.3 eV). However, the second reaction step almost completely offsets this difference in energetic cost, with a) requiring 0 eV and b) needing 0.8 eV for the epoxide formation reaction. These results are so far rather unsurprising, as in the absence of any surface for the carbonate to bind to or the reactants to adsorb on, we can expect neither the assumed driving force (the $Na_2CO_3$ formation) nor any overall energetic difference between the two reaction pathways, due to both educts having almost the same heat of formation. One aspect that we have neglected within our calculations so far is the influence of the zero-point-energy. While the influence of the zero-point-energy is often neglected because it is comparatively small, it can significantly impact chemical reactions, particularly in which multiple bonds are broken/ created. We performed frequency calculations for the vacuum reaction and were able to confirm that for the reactions in question, the change in zero-point-energy is relatively low, with the most significant change of any reaction step being 0.13 eV and the zero-point-energy influence over the complete PO formation reactions being no higher than 0.03 eV, which is far below the zero-point-energy of a typical C–H bond of 0.2–0.3 eV.[44] Progressing to the surface reactions, we find both exothermic and endothermic reaction steps. A list of all reaction energies is compiled in Table 2. We found the carbonate-producing reaction (Step 1) to be exothermic on all tested surfaces except the NaCl(100) surface. However, the PO formation step (Step 2) was endothermic on all surfaces except the NaCl(100) surface. In particular, most surfaces did not exhibit a reaction path without at least one step energy over 1 eV.

**Table 2.** Calculated reaction energies for the proposed PO formation reaction on all considered sodium and sodium chloride surfaces.

| | Step 1 | Step 2 | Total |
|---|---|---|---|
| Na(100) a) | −1.62 eV | +1.43 eV | −0.19 eV |
| Na(100) b) | −0.53 eV | +1.18 eV | +0.65 eV |
| Na(110) a) | −0.31 eV | +1.10 eV | +0.79 eV |
| Na(110) b) | −0.39 eV | +1.86 eV | +1.47 eV |
| Na(111) a) | −5.24 eV | +1.89 eV | −3.35 eV |
| Na(111) b) | −0.74 eV | +1.72 eV | +0.98 eV |
| NaCl(100) a) | +3.02 eV | −2.56 eV | +0.46 eV |
| NaCl(100) b) | −0.35 eV | +0.83 eV | +0.48 eV |
| NaCl(111) a) | −1.38 eV | +1.92 eV | +0.54 eV |
| NaCl(111) b) | −0.94 eV | +1.50 eV | +0.56 eV |

Consequently, it is unlikely that the whole reaction occurs on any one surface. However, a possible reaction path is found if one considers the non-static nature of the forming SEI. Assuming that reaction step 1 occurs on newly exposed sodium metal or a sodium-rich surface, the intermediate propanolates should readily form. During the decomposition of the perchlorate-containing electrolyte, the initial sodium metal surfaces transform into increasingly chloriderich surface structures. Upon this chlorination of the sodium surfaces, the adsorbed propanolate is destabilized, resulting in the ring-closing reaction leading to the formation of propylene oxide which is stabilized by the eventually forming sodium chloride. Figure 12 depicts the proposed reaction pathway for the formation of PO in a PC and $NaClO_4$ containing electrolyte. In the construction of this scheme we have been guided by the experimentally based assumption[45] that the discharge products in almost all cases are either sodium peroxide, $Na_2O_2$, or sodium superoxide, $NaO_2$. This ongoing SEI formation reaction and Na-metal exposure to the electrolyte is supported by the consistently increasing pressure during long-term storage experiments, demonstrating constant CO formation.[25] It is important to note that within this work, we focus on the thermodynamics of the proposed reaction pathway. One would also have to consider the kinetics to understand the reaction completely. A proper study including nudged elastic band (NEB) calculations was deemed beyond the scope of this work, however. Furthermore, while this work focuses on the interaction of electrolyte molecules with the sodium metal interface, at later stages of the SEI formation other mechanisms could come into play, e.g. an electron transfer through the SEI film as proposed recently.[46,47] In the following section, we employed XPS measurements to investigate the interphase between sodium metal and our electrolyte mixtures to confirm or disprove the presence of NaCl in the interphase.

## XPS Measurements

To better understand the correlation between theoretical DFT calculations and experimental GC measurements, surface characterization to detect solid decomposition products was performed using XPS. Herein, we investigated the effect of storage time and liquid composition on the surface layer of sodium metal by exposing the metal to PC and the PC-based electrolyte mixtures comprising the electrolyte salt $NaClO_4$ without and with 10% VC. The spectra of the pristine Na metal surface are shown in the supporting information (Figure S1). Two samples were prepared with short exposure times of 2 min and 4 min. The two short exposure times did not show significant differences in the surface composition. Data for the 4 min exposure is thus only provided in the supporting information (Figures S3–S6). Another Na metal sample was exposed to the three liquids for 2 hours. To provide a clear

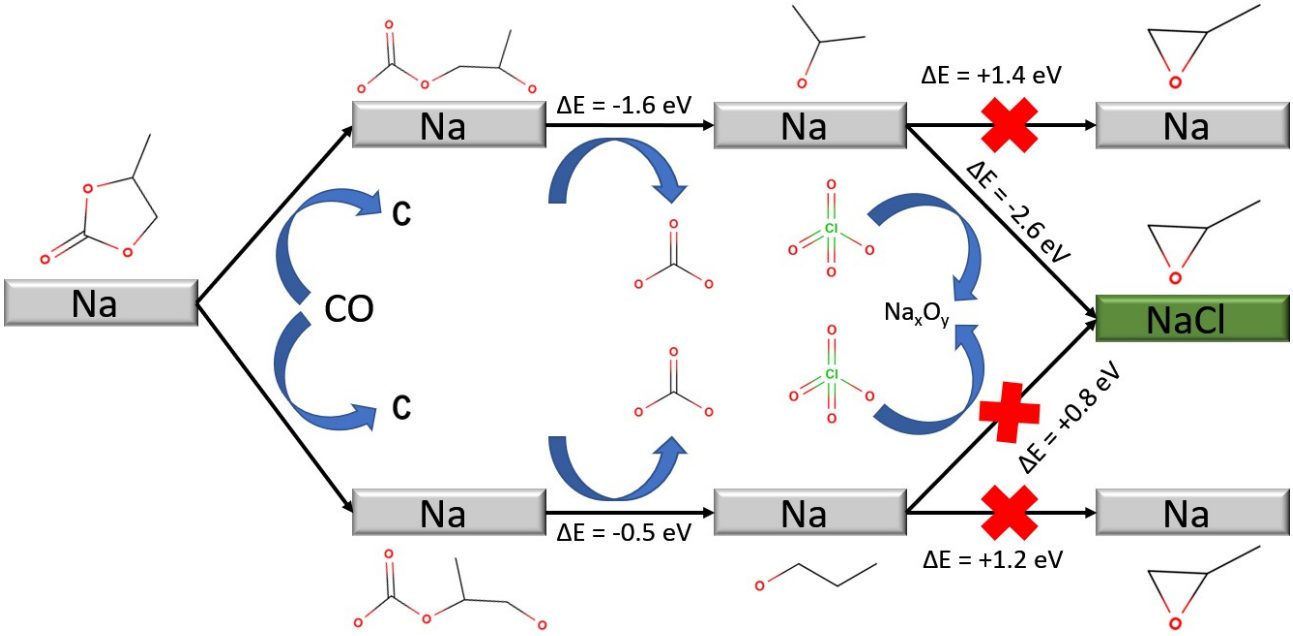


**Figure 12.** Reaction scheme for the proposed PO formation pathway, perchlorate decomposition leads to increasingly chloride-rich surfaces, which enable the ring-closing reaction for decomposition products of PC previously formed on the metal surface.

presentation and more comparable spectra, the intensity was normalized, setting the maximum peak height to 1.

### *C 1s Spectra*

The C 1s spectrum for Na submerged in pure PC solvent (Figure 13a) shows three large peaks at binding energies of 285.0 eV (C–C, C–H), 286.4 eV (C–O) and 290.4 eV ($CO_3$) in relative intensities of 1.5 : 2 : 1 (for 2 min). These binding energies and relative intensity ratios are close to the observed values for liquid PC measured using near ambient pressure XPS indicating either adsorbed PC or initial reactions that do not significantly change carbon nearest neighbor configurations.[48] In addition, a peak at 287.7 eV is observed. This binding energy may be expected for carbon in a carbonyl group (C=O). In the case of pure PC, there are two carbonate species found, one from the PC solvent itself at 290.4 eV and one from $Na_2CO_3$ at 289.3 eV. After storing a Na metal electrode in PC for 2 h, the same PC-attributed peaks can still be observed (Figure 13b). However, the intensity ratio between the three main peaks (CC, C–H/C–O/$CO_3$) changes from 1.5 : 2 : 1 for the 2 min. to 2.8 : 1.6 : 1 for 2 h indicating further reactions between the Na surface and PC. Compared to the pure metal this amount of $CO_3$ is not found (less than 1 atom-%). Also, the pristine metal has a significantly higher proportion of C–C/C–H (47 atom-%). Spectra of the pristine Na metal surface are shown in the supporting information (Figure S1). This indicates that the $CO_3$ species is formed on the surface after the addition of PC. The data presented in Figure 13 corresponds to C 1s spectra for Na metals submerged in $NaClO_4$-containing electrolytes, either without (c, d) or with VC as additive (e, f). For all these samples with the addition of salt, the spectra show prominent peaks at approximately 285 eV and 289 eV with two less intense peaks at around 286.3 eV and 287.5 eV. The peak with the highest binding energy at 289.3 eV peak is assigned to $Na_2CO_3$.[49] The peak at 287.5 eV is assigned to C=O and (C=O)O environments contained for example in $HCO_2Na$, while the peaks at lower binding energies of 286.3 eV and 285 eV indicate C–O and C–C/C–H bonds, respectively. As no PC-carbonate peak at 290.4 eV is observed anymore, the peak at 286.3 eV could be attributed to reacted solvent products such as carbon in –CONa indicating an alkoxide species like $CH_3ONa$ or $CH_3CH_2ONa$ while the corresponding O 1s peak was observed at 531.7 eV.

### *O 1s Spectra*

The O 1s spectra of Na metal dipped in pure PC show two main features at binding energies 531.3 eV and 532.7 eV in a relative intensity ratio of 1 : 1 (for 2 min., Figure 13a) and 1 : 2 (for 2 h, Figure 13b). Combined, the O 1s and C 1s signature peaks fit the ones expected from the molecular structure of the PC molecule, three chemically different carbon positions and two chemically different oxygen positions. The observed intensity ratios do not match perfectly because, as discussed in the C 1s section, some $Na_2CO_3$ and other reaction products between Na and PC have formed on the surface. Generally, the O 1s region overlaps partially with the Na Auger region when using 1486.6 eV as excitation energy in XPS. Therefore, all O 1s spectra include two characteristic Auger peaks for sodium at 524 eV and 536 eV. When moving from the Na metal submerged in pure PC to Na metal in electrolytes based on $NaClO_4$ in PC without (Figure 13c, d) and with VC (Figure 13e, f) the shape of the O 1s spectra changes significantly indicating more pronounced reactions between the metal surface and the electrolytes than

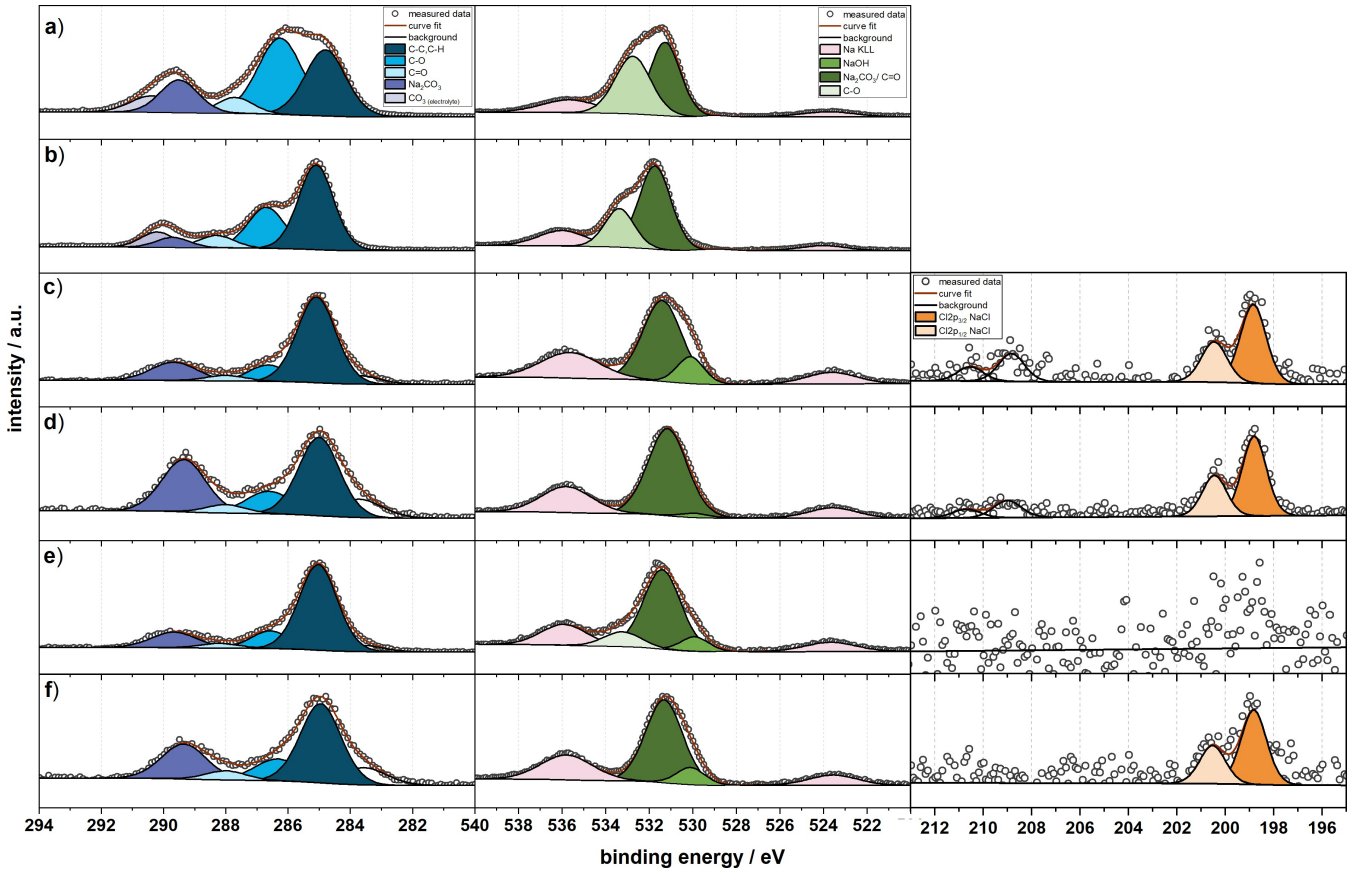


**Figure 13.** C 1s, O 1s and Cl 2p spectra of the sodium surfaces after storage in different electrolytes: pure PC solvent for 2 min (a) and 2 h (b), 0.75 M PC $NaClO_4$ for 2 min (c) and 2 h (d), 0.75 M PC-VC $NaClO_4$ for 2 min (e) and 2 h (f). The binding energy scale is calibrated versus the hydrocarbon peak at 285 eV.

between the metal surface and the pure solvent. The prominent O 1s peaks around 531 eV could be fitted with three components. For both samples submerged for only two minutes, a clear peak at low binding energies is observed. This peak at 530.0 eV is attributed to NaOH. The main peak centered at 531.1 eV is assigned to a carbonate species such as contained in $Na_2CO_3$ and alkyl carbonates. Because the intensity of this peak in the O 1s for carbonate is too high in relation to the $-CO_3$ peak in the C 1s, this indicates that there is likely another species contributing to this peak. As observed in the C 1s this could indicate alkoxide species like $CH_3ONa$, leading to an O 1s peak at 531.7 eV binding energy. After considering the alkoxide species contribution to the peak intensity at 531.1 eV, the relative amount of oxygen from the $CO_3$ peak is in good agreement with the C 1s peak for $Na_2CO_3$.

### *Cl 2p Spectra*

Cl 2p emissions were observed for the samples containing $NaClO_4$ as electrolyte salt. In the case of Na metal soaked in 1 M $NaClO_4$ in PC for 2 min and 2 h, the Cl 2p spectra show two doublet peaks at 198.7 eV and 209.5 eV which correspond to NaCl and $NaClO_4$.[50] Thus, even with the described washing procedure, there was a small residual amount of conductive salt left on the surface. The atomic percentage for $NaClO_4$ is lower than 0.1% and therefore not included in the following evaluation. Interestingly, in the case of the electrolytes without VC as additive (Figure 13c, d), a strong NaCl contribution is observed, indicating electrolyte salt decomposition. When VC is used in the electrolyte (Figure 13e, f), initially, after 2 min soaking, no clear NaCl signal is observed while after 2 h, there is a NaCl contribution.

### SEI Composition in Different Electrolyte Mixtures

For a quantitative analysis of the surface composition, the atomic concentrations (atom-%) for elements and specific components were derived from the peak areas of the curvefitted spectra (Figure 13) and on basis of the instrument specific Scofield factors. The overall elemental composition is summarized in Table 3 and Figure 14. The various sodium salts typical for SEI components (e.g. $Na_2CO_3$, NaCl, R-ONa, NaOH) are summarized as "Na1s", as their binding energies fall in the same range.

We generally observe that the amount of reaction products on the Na electrode surfaces increases with increasing storage time. The presented data also shows an increased reactivity between the Na electrode surfaces and the respective liquids

when the electrolyte salt is included. The elements present on the Na metal surface after soaking in $NaClO_4$ containing electrolyte with and without VC indicate that both electrolyte solvent and salt electrolyte salt contribute towards SEI formation. High oxygen and carbon concentrations confirm the assumption that solvent reduction is the major reaction pathway forming the SEI. However, the rise in Na species concentration when switching from pure solvent to electrolytes with conductive salt indicates that more Na-containing organic and inorganic SEI species are formed. During the decomposition of the perchlorate-containing electrolyte (without VC), the initial sodium metal surfaces is rendered increasingly chloride-rich through the formation of NaCl (Figure 13c, d). $NaClO_4$ reduction presumably also produces surface oxides, which have not been observed herein. However, the presence of NaOH could indicate conversion of sodium oxides in presence of residual $H_2O$ in the electrolyte. The water contents between 26.5 and 31.3 ppm, would probably only account for a fraction of the NaOH species seen in the O 1s spectra. Interestingly, the initial chloride content (after 2 min) is lower when 10% VC is added to the electrolyte. Although the chloride content increased after 2 h in the VC-containing electrolyte as well, its relative amount compared to the VC-free electrolyte is negligibly small. This indicates that VC as an additive has an inhibiting effect on the electrolyte salt decomposition and thus reduces both the amount of chloride at the sodium surface and as a result suppresses the PO evolution reaction.

**Table 3.** Elemental quantification of surface layers on Na metal electrodes treated with different electrolytes for different time periods.

| Composition | C 1s Content/ atomic-% | O 1s Content/ atomic-% | Cl 2p Content/ atomic-% | Na 1s Content/ atomic-% |
|---|---|---|---|---|
| PC 2 min | 49.3 | 37.6 | – | 13.0 |
| PC 2 h | 57.0 | 32.5 | – | 10.5 |
| PC/$NaClO_4$ 2 min | 40.0 | 32.1 | 0.65 | 27.2 |
| PC/$NaClO_4$ 2 h | 24.0 | 36.9 | 1.18 | 38 |
| PC-VC/$NaClO_4$ 2 min | 46.0 | 33.2 | 0.17 | 20.6 |
| PC-VC/$NaClO_4$ 2 h | 31.0 | 36.3 | 0.5 | 32.3 |

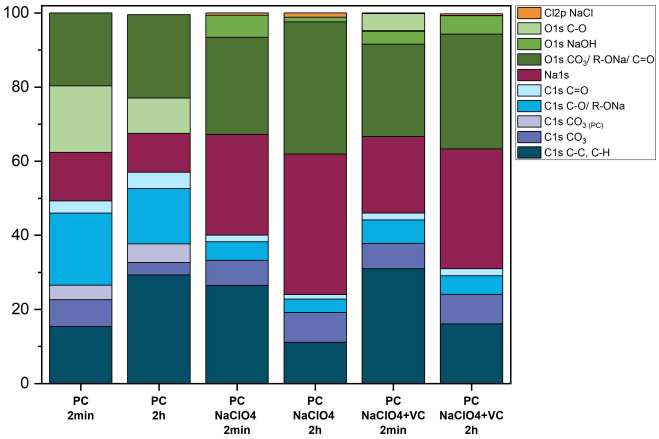


**Figure 14.** Bar plots of the atomic concentration found for the different storage conditions forming the SEI components by XPS.

### Alternative PO formation mechanisms

As mentioned, our proposed PO formation pathway (see Figure 12) is far from being the only possible reaction pathway. We compared common synthesis methods for ethylene oxide and propylene oxide and selected further candidate reactions for the PO formation within our experiments. All reactions requiring an aqueous environment and specific catalysts were dismissed, as neither were present in our experiments. We identified three further reaction mechanisms that could be considered within our setup. First, we look at the direct oxidation of ethene used to synthesize ethylene oxide according to Eq. (3).[51]

$$7\,CH_2 = CH_2 + 6\,O_2 \rightarrow 6\,(CH_2CH_2)O + 2\,CO_2 + 2\,H_2O \quad (3)$$

We can, of course, apply this reaction mechanism to the propene gas within our experiments. The formation of propene gas during PC decomposition has been demonstrated in previous simulations and experimental measurements as well as in our study, as shown in the GC section.[52,33] While the formation of excess oxygen is far from impossible due to the presence of oxygen-rich perchlorate, this reaction mechanism would result in carbon dioxide, which our experiments do not detect, ruling out this reaction path. A second possibility is the chlorination of propene gas, leading to a follow-up reaction with a sodium oxide surface. An equivalent reaction for ethylene oxide is shown in Eq. (4), followed by Eq. (5).

$$CH_2 = CH_2 + Cl_2 \rightarrow Cl{-}CH_2CH_2{-}Cl \quad (4)$$

$$Cl{-}CH_2CH_2{-}Cl + Na_2O \rightarrow (CH_2CH_2)O + 2\,NaCl \quad (5)$$

While chloride ions are present in the electrolyte, the chlorination of propene is unlikely in the absence of chlorine gas. Further, we could not detect chlorine gas or any chlorinated intermediate. The third reaction is a surface oxidation of the propandiolate formed during the initial decomposition of PC under CO formation, mentioned in Eq. (6).

$$O{-}CH_2{-}CH_2{-}O + 2\,Na \rightarrow (CH_2CH_2)O + Na_2O \quad (6)$$

This reaction cannot be dismissed, as all necessary educts and products have been detected experimentally or theoretically. We, therefore, replicated our approach for the PO formation mechanism on sodium with the surface oxidation process. We found the initial surface oxidation step to be endothermic on all tested sodium surfaces (Table 4). The reaction schematic for the surface oxidation pathway is depicted in Figure 15, and the PO formation reaction along this path would require over 2 eV in total. The direct surface oxidation is energetically unfavorable compared to our proposed carbonate formation, supporting the initial claim that carbonate formation is the driving force behind the first step of the PO formation mechanism. Further, a reaction of PC into PO

**Table 4.** Calculated reaction energies for the direct surface oxidation mechanism on all considered sodium surfaces.

| | Step 1 | Step 2 | Total |
|---|---|---|---|
| Na(100) a) | +0.81 eV | +1.43 eV | +2.24 eV |
| Na(100) b) | +1.06 eV | +1.18 eV | +2.24 eV |
| Na(110) a) | +1.86 eV | +1.10 eV | +2.96 eV |
| Na(110) b) | +1.10 eV | +1.86 eV | +2.96 eV |
| Na(111) a) | +4.78 eV | +1.89 eV | +6.67 eV |
| Na(111) b) | +4.95 eV | +1.72 eV | +6.67 eV |

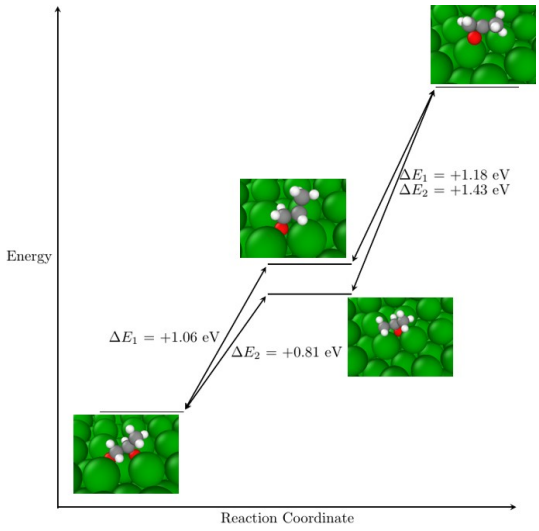


**Figure 15.** Reaction scheme for propylene oxide formation using the surface oxidation reaction pathway, all reaction steps are highly endothermic.

resulting in $CO_2$ formation has been proposed.[53] Similarly to the direct oxidation reaction of propene, we dismiss this reaction due to the absence of $CO_2$ in our measurements.

Finally, one has to consider the possibility that the PO formation might occur not on the surface but inside the electrolyte. A reaction in which perchlorate acts as an oxidizing agent and oxidizes the readily formed propene gas is certainly possible. However, perchlorate ions are generally not very redox-active in solution.[54] Further, the reduction of $NaClO_4$ would have to lead to the formation of either $NaClO_3$, which by itself tends to disproportionate into $NaClO_4$ and NaCl or $O_2$, which should lead to the oxidation of CO into $CO_2$ within our system due to the abundance of CO present. Due to the absence of $CO_2$ in our measurements, the $O_2$ generation is deemed unlikely. While sundering one oxygen from the perchlorate would provide the oxygen required for the oxidation of propene, the perchlorate ion reduction to chlorate usually required biological processes.[55] Further, in order to initiate any oxidation reaction, the propene molecule would have to penetrate the solvation shell around the perchlorate ions in solution, which should significantly hinder the kinetics of such a reaction.

## Conclusions

This work showcased a combined theoretical and experimental approach toward understanding the initial degradation steps leading to forming the solid electrolyte interphase in sodium batteries. We were able to link the different scales, both in terms of size and time, between atomistic scale modeling and gas chromatography by correlating the adsorption behavior of decomposition products with their detectability within the GC setup. We further showed that AIMD simulations spanning just a few ps, depicting perchlorate decomposition on alkali metal surfaces and initial stages of phase separation, could be extrapolated and confirmed by X-ray photoelectron spectroscopy. By combining the insights gained from experimental measurements and theoretical simulations, we could not only identify changes in the decomposition process of the electrolyte but also propose a possible mechanism by which these changes occur. Specifically, we explain the sudden formation of propylene oxide upon adding sodium perchlorate into an electrolyte containing propylene carbonate in contact with a sodium metal surface. This formation was found to be linked to NaCl appearing on the sodium metal, which in turn enables a ring-closing reaction for the readily formed precursor of PO. The precursor was found to be driven by a carbonate-forming reaction rather than an oxide-forming reaction. The abundance of sodium carbonate and sodium chloride within the XPS measurements supports these findings. This study provides an initial step to understand electrolyte decomposition, it provides detailed mechanistic insights that may be applicable beyond the scope of this electrolyte-salt combination. Further work on the effects on performance and lifetime is needed, though. The formation of inorganic compounds, such as fluorides or carbonates, within the SEI of alkali metal batteries and their direct impact on the stability of the SEI through properties like solubility or elasticity is well established. However, secondary effects of such evolving structures, like the sudden formation of epoxides, as shown in this study, still need to be further understood. The appearance of additional electrolyte decomposition products should not be underestimated since molecules like epoxides can enable polymerization reactions[56] and lead to significant changes in the structure and properties of the SEI.

## Experimental

### Computational Details

All reactions were modeled using ab initio DFT calculations within the plane-wave-based Vienna ab initio simulation package (VASP)[57] framework. The exchange-correlation was calculated using the revised Perdew–Burke–Ernzerhof functional (RPBE)[58] to better account for chemisorption. The electron-core interactions were described via a projector augmented wave (PAW) method.[59,60] A Γ centered 5×5×1 k-point grid was used to calculate the adsorption energies. The electronic self-consistent-field (SCF) was converged up to $10^{-6}$ eV using the Gaussian smearing scheme with a width of 0.05 eV, with the ionic geometry being converged to energetic differences below $10^{-5}$ eV. The DFT–D3 Van-der-Waals (vdW)

correction of Grimme[61] was applied to include dispersion effects during molecular adsorption. The molecular dynamics simulations simulated a canonical ensemble using the Nose algorithm with a Nose-frequency of $10^{14}$ Hz at a temperature of 300 K. The frequency calculations were computed using a finite differences approach with a displacement width of 0.015 Å to stay within the harmonic approximation. The surfaces were modeled using the slab model with (4×4) unit cells topped by a vacuum region with a height larger than 15 Å. The slab thickness varied between 4 to 6 layers, dependent on the specific surface. The minimum slab thickness was 9 Å.

Interactions between the adsorbate and the electrolyte were neglected within the scope of this work. Due to the absence of further electrolyte molecules within the simulation cell, solvation effects cannot be caught, and adsorption energies are likely to be overestimated with respect to any system in which electrolyte is present. While the dispersion correction was included to archive a physically more correct description of the system,[62] in the absence of any electrolyte solvent, this might further contribute to the overestimation of the adsorption energies with respect to the real system. In order to evaluate the effect of the dispersion correction, a comparison between the adsorption energies of a selection of adsorbates on the Na(100) surface calculated with and without the D3 dispersion correction was made, see Table S2. The dispersion correction led to an increase in the adsorption energy between 0.2 eV for PO to 0.66 eV for $C_4H_6O_4$.

## GC

Gas formation was investigated in an EL-CELL (PAT-Cell-Press) with a cup (polypropylene) containing the electrolyte mixture and sodium pieces. The cell was handled in an argon filled glove box and a PEEK sealing was used to close the cell tightly. The pressure was observed over a period of time and afterward the gases were extracted with a gastight syringe. The procedure is described in Ref. [25] in more detail.

Gas analyses were carried out using a Clarus 690 gas chromatograph (Perkin Elmer, USA), which was additionally equipped with an ARNEL 4019 system (Perkin Elmer, USA) and a mass spectrometer (MS, SQ8S, Perkin Elmer, USA). The gas sample was injected using a syringe into the gas injection system, which was connected to multiple separation columns and injectors (thermal conductivity detectors (TCD) and mass spectrometer (MS)). The gas samples were introduced at room temperature and then switched to the columns. The setup allowed the detection and quantification of the gases $CO_2$, CO, $CH_4$, $C_2H_2$, $C_2H_4$, $C_2H_6$, $O_2$, He and Ar from a concentration of about 150 ppm. Propylene oxide and volatile solvents were detected with the MS detector. Evaluation and control were performed using TurboMass software (6.1.2.2048, Perkin Elmer, USA).

## XPS

The X-ray photoelectron spectroscopy measurements were performed using a K-alpha spectrometer (Thermo Fisher Scientific, East Grinstead, UK), applying a micro-focused, monochromatized Al Kα X-ray source ($h\nu = 1486.6$ eV) with 400 μm spot size. The metal electrodes (supported by the spacer) were placed on a sample holder using copper tape and transferred without exposure to air or moisture to an Ar-filled glovebox connected to the spectrometer. In case of localized surface charging, the binding energy shifts were minimized using the K-Alpha charge compensation system during analysis, using a electron flood gun as charge compensation with low energy-electrons of 8 eV kinetic energy and Ar ions with low energy. Data acquisition and processing was carried out using the Thermo Avantage software (Version 5.9922, Thermo Scientific). All spectra were referenced to the hydrocarbon C 1s peak (C–C, C–H) at 285.0 eV while the overall binding energy scale was controlled by means of the well-known photoelectron peaks of metallic Cu, Ag, and Au, respectively. On each sample surface, a full set of spectra was aquired from at least two different spots, using a step size of 0.1 eV and a pass energy of 50 eV for the detailed spectra. For intense peaks and/or peaks clearly evidenced by the peak shape, the binding energy uncertainty was set around ±0.1 eV during curve fitting. In case of weak peaks and no direct justification by the peak shape, the uncertainty was set to ±0.2 eV. Spectral changes due to X-ray radiation exposure was checked via repeated measurements but was not observed. The analyzer transmission function, Scofield's sensitivity factors, and effective attenuation lengths for photoelectrons were applied for quantification. Effective attenuation lengths were calculated using the standard TPP-2 M formalism. Core peaks were analyzed using the "smart background" (nonlinear Shirley-type background with an additional constraint that the background function is not greater than any datapoint in the measured region). For peak fitting, Voigt profiles were used with a 70% Gaussian and 30% Lorentzian contribution. To provide a clear presentation and more comparable spectra, the intensity was normalized setting the maximum peak height to 1.

## Electrolyte Preparation

0.75 M $NaClO_4$ (Alfa Aesar, anhydrous, ACS, 98.0–102.0%) was dissolved in 1) DEC:EC (Sigma–Aldrich, anhydrous ≥99%; Sigma–Aldrich, anhydrous 99%) 50:50 by volume and 2) PC (Sigma–Aldrich, anhydrous 99.7%) and stirred in high-density polyethylene vials overnight at room temperature. A third electrolyte was prepared by adding 10% VC (Thermo Scientific Chemicals, 98%) by volume to the 0.75 M $NaClO_4$ in PC electrolyte.The water content on the pure solvent and the electrolyte with and without additive was determined by Karl–Fischer–Titration. Each experiment was carried out three times and the values were averaged. For PC a water content of 26.5 ppm was found. For PC-based electrolyte mixtures the water content was 26.1 ppm (0.75 M $NaClO_4$) and 31.3 ppm (0.75 M $NaClO_4$ + 10% VC).

## Metal submerging Experiments

Samples were prepared in an Ar-filled glovebox ($O_2$ < 0.1 ppm, $H_2O$ < 0.1 ppm). The Na metal (Sigma–Aldrich, 99.9% trace metals basis) which was delivered in mineral oil was first washed in hexane and then placed and rolled out using a protective PE (polyethylene) sheet to reduce sticking to the rolling pin and contamination's on a stainless-steel spacer. The samples were placed in high-density polyethylene vials with 1 mL of the three electrolytes mention above and stored in the electrolytes for 2 minutes, 4 minutes and 2 hours, respectively. After storage, the Na electrodes were washed twice by immersion for 2 minutes in a glass vial containing 3 mL of DEC or PC and dried under vacuum. These conditions are based on a pre-study investigating the washing conditions and it was found that this procedure removes almost all residual conductive salt.-Furthermore, reference samples of NaCl and pristine Na were measured (see supporting information), where NaCl powder was mounted to the sample holder by pressing the powder into conductive double sided carbon tape.

## Acknowledgements

This work contributes to the research performed at CELEST (Center for Electrochemical Energy Storage Ulm-Karlsruhe) and was funded by the Deutsche Forschungsgemeinschaft (DFG, German Research Foundation) under Germany's Excellence Strategy – EXC 2154 – Project number 390874152. The authors furthermore acknowledge computer time supplied by the state of Baden-Württemberg through the bwHPC project and the Germany Research Foundation (DFG) through grant number INST 40/467-1 FUGG (JUSTUS cluster). Open Access funding enabled and organized by Projekt DEAL.

## Conflict of Interests

The Authors declare no Conflict of Interest.

## Data Availability Statement

The data that support the findings of this study are available from the corresponding author upon reasonable request.

**Keywords:** Na-ion batteries · electrolyte decomposition · solid-electrolyte interphase · density functional theory · X-ray photoelectron spectroscopy and gas chromatography

[1] R. Schlögl, *ChemSusChem* **2010**, *3*, 209.
[2] S. Choi, G. Wang, *Adv. Mater. Technol.* **2018**, *3*, 1700376.
[3] M. L. Vera, W. R. Torres, C. I. Galli, A. Chagnes, V. Flexer, *Nat. Rev. Earth Environ.* **2023**, *4*, 149.
[4] Y. Ma, Y. Ma, H. Euchner, X. Liu, H. Zhang, B. Qin, D. Geiger, J. Biskupek, A. Carlsson, U. Kaiser, A. Groß, S. Indris, S. Passerini, D. Bresser, *ACS Energy Lett.* **2021**, *6*, 915.
[5] S. Ye, L. Wang, F. Liu, P. Shi, Y. Yu, *eScience* **2021**, *1*, 75.
[6] B. Tang, Y. Zhao, Z. Wang, S. Chen, Y. Wu, Y. Tseng, L. Li, Y. Guo, Z. Zhou, S.-H. Bo, *eScience* **2021**, *1*, 194.
[7] J. W. Choi, D. Aurbach, *Nat. Rev. Mater.* **2016**, *1*, 16013.
[8] H. Euchner, A. Groß, *Phys. Rev. Mater.* **2022**, *6*, 040302.
[9] C. Bao, B. Wang, P. Liu, H. Wu, Y. Zhou, D. Wang, H. Liu, S. Dou, *Adv. Funct. Mater.* **2020**, *30*, 2004891.
[10] J. Lee, Y. Lee, J. Lee, S.-M. Lee, J.-H. Choi, H. Kim, M.-S. Kwon, K. Kang, K. T. Lee, N.-S. Choi, *ACS Appl. Mater. Interfaces* **2017**, *9*, 3723.
[11] J. Zhang, J. Yang, L. Yang, H. Lu, H. Liu, B. Zheng, *Mater Adv* **2021**, *2*, 1747.
[12] R. Gond, W. van Ekeren, R. Mogensen, A. J. Naylor, R. Younesi, *Mater. Horiz.* **2021**, *8*, 2913.
[13] P. Bharathy S, L. Brett, *J. Electrochem. Soc.* **2018**, *165*.
[14] M. Goktas, C. Bolli, J. Buchheim, E. J. Berg, P. Novák, F. Bonilla, T. Rojo, S. Komaba, K. Kubota, P. Adelhelm, *ACS Appl. Mater. Interfaces* **2019**, *11*, 32844.
[15] X. Zhou, P. Li, Z. Tang, J. Liu, S. Zhang, Y. Zhou, X. Tian, *Energies* **2021**, *14*.
[16] J. Fondard, E. Irisarri, C. Courrèges, M. R. Palacin, A. Ponrouch, R. Dedryvère, *J. Electrochem. Soc.* **2020**, *167*, 070526.
[17] Y. Xu, H. Wu, Y. He, Q. Chen, J.-G. Zhang, W. Xu, C. Wang, *Nano Lett.* **2020**, *20*, 418.
[18] Z. Peng, X. Cao, P. Gao, H. Jia, X. Ren, S. Roy, Z. Li, Y. Zhu, W. Xie, D. Liu, Q. Li, D. Wang, W. Xu, J.-G. Zhang, *Adv. Funct. Mater.* **2020**, *30*, 2001285.
[19] K. Li, J. Zhang, D. Lin, D.-W. Wang, B. Li, W. Lv, S. Sun, Y.-B. He, F. Kang, Q.-H. Yang, L. Zhou, T.-Y. Zhang, *Nat. Commun.* **2019**, *10*, 725.
[20] B. Rowden, N. Garcia-Araez, *Energy Reports* **2020**, *6*, 10.
[21] S.-J. Yang, N. Yao, X.-Q. Xu, F.-N. Jiang, X. Chen, H. Liu, H. Yuan, J.-Q. Huang, X.-B. Cheng, *J. Mater. Chem. A* **2021**, *9*, 19664.
[22] H. Zhang, D. Wang, C. Shen, *Appl. Surf. Sci.* **2020**, *507*, 145059.
[23] J. He, H. Wang, Q. Zhou, S. Qi, M. Wu, F. Li, W. Hu, J. Ma, *Small Methods* **2021**, *5*, 2100441.
[24] A. J. Naylor, M. Carboni, M. Valvo, R. Younesi, *ACS Appl. Mater. Interfaces* **2019**, *11*, 45636, pMID: 31718143.
[25] A. Hofmann, Z. Wang, S. P. Bautista, M. Weil, F. Müller, R. Löwe, L. Schneider, I. U. Mohsin, T. Hanemann, *Electrochim. Acta* **2022**, *403*, 139670.
[26] P. W. Tasker, *Phil. Mag. A* **1979**, *39*, 119.
[27] K. Saiki, A. G. A. Goda, A. K. A. Koma, *J. Appl. Phys.* **1997**, *36*, L55.
[28] J.-Y. Chung, H.-D. Li, W.-H. Chang, T. C. Leung, D.-S. Lin, *Phys. Rev. B* **2011**, *83*, 085305.
[29] A. G. Kvashnin, D. G. Kvashnin, A. R. Oganov, *Scientific Rep.* **2019**, *9*, 2045.
[30] A. Groß, *Curr. Opin. Electrochem.* **2023**, *37*, 101170.
[31] S. Sakong, C. Mosch, A. Groß, *Phys. Chem. Chem. Phys.* **2007**, *9*, 2216.
[32] W. Jin, Y. Wang, T. Liu, C. Ding, H. Guo, *Appl. Surf. Sci.* **2022**, *599*, 154024.
[33] D. Stottmeister, A. Groß, *Batteries & Supercaps* **2023**, *6*, e202300156.
[34] G. Hernandez, R. Mogensen, R. Younesi, J. Mindemark, *Batteries & Supercaps* **2022**, *5*, e202100373.
[35] A. Hofmann, Z. Wang, S. P. Bautista, M. Weil, F. Müller, R. Löwe, L. Schneider, I. U. Mohsin, T. Hanemann, *Data in Brief* **2022**, *40*, 107775.
[36] Q. Liu, D. Mu, B. Wu, L. Wang, L. Gai, F. Wu, *ChemSusChem* **2017**, *10*, 786.
[37] Q. Liu, D. Mu, B. Wu, H. Xu, L. Wang, L. Gai, L. Shi, F. Wu, *J. Electrochem. Soc.* **2017**, *164*, A3144.
[38] G. Zhuang, Y. Chen, P. N. Ross, *Surf. Sci.* **1998**, *418*, 139.
[39] J. Yu, P. B. Balbuena, J. Budzien, K. Leung, *J. Electrochem. Soc.* **2011**, *158*, A400.
[40] K. Leung, F. Soto, K. Hankins, P. B. Balbuena, K. L. Harrison, *J. Phys. Chem. C* **2016**, *120*, 6302.
[41] R. Mogi, M. Inaba, Y. Iriyama, T. Abe, Z. Ogumi, *J. Power Sources* **2003**, *119–121*, 597, selected papers presented at the 11th International Meeting on Lithium Batteries.
[42] G. V. Zhuang, K. Xu, H. Yang, T. R. Jow, P. N. Ross, *J. Phys. Chem. B* **2005**, *109*, 17567.
[43] D.-H. Kim, B. Kang, H. Lee, *J. Power Sources* **2019**, *423*, 137.
[44] A. Govender, D. C. Ferré, J. W. H. Niemantsverdriet, *ChemPhysChem* **2012**, *13*, 1591.
[45] P. Adelhelm, P. Hartmann, C. L. Bender, M. Busche, C. Eufinger, J. Janek, *Beilstein J. Nanotechnol.* **2015**, *6*, 1016.
[46] K. Leung, *Phys. Chem. Chem. Phys.* **2020**, *22*, 10412.
[47] K. Leung, L. C. Merrill, K. L. Harrison, *J. Phys. Chem. C* **2022**, *126*, 8565.
[48] J. Maibach, I. Källquist, M. Andersson, S. Urpelainen, K. Edström, H. Rensmo, H. Siegbahn, M. Hahlin, *Nat. Commun.* **2019**, *10*, 3080.
[49] L. Caracciolo, L. Madec, H. Martinez, *ACS Appl. Energ. Mater.* **2021**, *4*, 11693.
[50] Y.-C. Lin, Y.-Y. Chen, B.-Y. Yu, W.-C. Lin, C.-H. Kuo, J.-J. Shyue, *Analyst* **2009**, *134*, 945.
[51] P. Kilty, W. Sachtler, *Catal. Rev. Sci. Eng.* **1974**, *10*, 1.
[52] H. Zhao, S.-J. Park, F. Shi, Y. Fu, V. Battaglia, P. N. Ross, G. Liu, *J. Electrochem. Soc.* **2013**, *161*, A194.
[53] L. Xing, C. Wang, W. Li, M. Xu, X. Meng, S. Zhao, *J. Phys. Chem. B* **2009**, *113*, 5181.
[54] G. M. Brown, *J. Electroanal. Chem.* **1986**, *198*, 319.
[55] G. B. Rikken, A. G. M. Kroon, C. G. van Ginkel, *Appl. Microbiol. Biotechnol.* **1996**, *45*, 420.
[56] Z. Liu, J. Huang, S. Chen, Y. Huang, F. Ding, W. Guo, D. Lei, L. Yang, F.-L. Qing, Z. You, *Int. J. Adhes. Adhes.* **2020**, *96*, 102456.
[57] G. Kresse, J. Furthmüller, *Phys. Rev. B* **1996**, *54*, 11169.
[58] B. Hammer, L. B. Hansen, J. K. Nørskov, *Phys. Rev. B* **1999**, *59*, 7413.
[59] P. E. Blöchl, *Phys. Rev. B* **1994**, *50*, 17953.
[60] G. Kresse, D. Joubert, *Phys. Rev. B* **1999**, *59*, 1758.
[61] S. Ehrlich, J. Moellmann, W. Reckien, T. Bredow, S. Grimme, *ChemPhysChem* **2011**, *12*, 3414.
[62] D. Mahlberg, S. Sakong, K. Forster-Tonigold, A. Groß, *J. Chem. Theory Comput.* **2019**, *15*, 3250.

Manuscript received: July 10, 2023
Revised manuscript received: October 11, 2023
Accepted manuscript online: October 11, 2023
Version of record online: November 17, 2023